

Synthesis of porous carbon from orange peel waste for effective volatile organic compounds adsorption: role of typical components

Qiaoyan Zhou^{1,2}, Huan Liu (✉)^{1,2}, Yipeng Wang³, Kangxin Xiao¹, Guangyan Yang¹, Hong Yao¹

1 School of Energy and Power Engineering, Huazhong University of Science and Technology, Wuhan 430074, China

2 Research Institute of Huazhong University of Science and Technology in Shenzhen, Shenzhen 518000, China

3 Universtar Science & Technology (Shenzhen) Co., Ltd., Shenzhen 518057, China

© Higher Education Press 2023

Abstract Volatile organic compounds have posed a serious threat to the environment and human health, which require urgent and effective removal. In recent years, the preparation of porous carbon from biomass waste for volatile organic compounds adsorption has attracted increasing attention as a very cost-effective and promising technology. In this study, porous carbon was synthesized from orange peel by urea-assisted hydrothermal carbonization and KOH activation. The role of typical components (cellulose, hemicellulose, and lignin) in pore development and volatile organic compounds adsorption was investigated. Among the three components, hemicellulose was the major contributor to high porosity and abundant micropores in porous carbon. Higher hemicellulose content led to more abundant –COOR, amine-N, and pyrrolic/pyridonic-N in the derived hydrochar, which were favorable for porosity formation during activation. In this case, the toluene adsorption capacity of the porous carbon improved from 382.8 to 485.3 mg·g⁻¹. Unlike hemicellulose, cellulose reduced the >C=O, amine-N, and pyrrolic/pyridonic-N content of the hydrochar, which caused porosity deterioration and worse toluene adsorption performance. Lignin bestowed the hydrochar with slightly increased –COOR, pyrrolic/pyridonic-N, and graphitic-N, and reduced >C=O, resulting in comparatively poor porosity and more abundant micropores. In general, the obtained porous carbon possessed abundant micropores and high specific surface area, with the highest up to 2882 m²·g⁻¹. This study can provide guidance for selecting suitable biomass waste to synthesize porous carbon with better porosity for efficient volatile organic compounds adsorption.

Keywords biomass waste, porous carbon, feedstock composition, urea-assisted hydrothermal carbonization, toluene adsorption, N-doped hydrochar

1 Introduction

In recent years, the dramatically increasing emission of volatile organic compounds (VOCs) has posed a serious threat to the environment and human health [1,2]. As one of the major hazards in the air, VOCs not only cause photochemical smog formation and ozone layer destruction but also harm human health because most are highly toxic and carcinogenic [3,4]. Therefore, it is urgent to develop effective techniques for VOCs removal. Among the VOCs removal methods, adsorption is considered to be an efficient and economic technology with the advantages of low energy consumption, facile operation process, and high VOCs recovery rate [5,6].

Activated carbon is the most widely used VOCs adsorbent due to its large specific surface area, abundant functional groups, and chemical stability [7,8]. Compared with coal-based materials and petroleum, the synthesis of porous carbon from biomass waste, e.g., coconut shell, mung bean husk, and fruit peels, has attracted much attention owing to its cheapness, abundance, and environmental friendliness [9,10]. Porous carbon is generally produced from biomass waste in two steps: carbonization and activation [11,12]. For biomass waste with high moisture content and complex compositions, hydrothermal carbonization (HTC) is suitable as pre-treatment since it does not require pre-drying and produces abundant oxygen-containing functional groups (OFGs) [13,14]. By activating the hydrochar, porous carbon with significantly better VOCs adsorption

performance can be obtained, which mainly relies on the enlargement of surface area and surface chemistry [15,16].

During the preparation process of porous carbon, the raw materials have a decisive influence on the structural properties and surface chemistry [17,18]. In this study, orange peel waste was used as the feedstock, of which hemicellulose, cellulose, and lignin were the main components. They undergo a series of different reactions in subcritical water and at low temperatures (150–350 °C) during HTC [19–21]. Cellulose and hemicellulose underwent a series of hydrolysis, dehydration, and polymerization. Finally, hydrochar with a hydrophobic core and hydrophilic shell was formed [22–24]. As for lignin, the non-dissolved lignin is transformed into the core of the hydrochar via solid–solid conversion, and the dissolved lignin decomposes to form phenolics as the shell [25,26]. Xiao et al. [27] pointed out that hemicellulose and cellulose increased the OFGs content, such as hydroxyl and ester. In contrast, the addition of lignin resulted in more benzene rings on the surface of hydrochar. Jain et al. [28] demonstrated that the enhanced OFGs in the hydrochar increased the mesoporous surface area of porous carbon by 100%. Obviously, the varying chemical compositions of feedstock play an essential role in the physicochemical properties of hydrochar, which further influence the porosity development in subsequent activation [19,29].

In addition to improving the VOCs adsorption effect by increasing the porosity, heteroatom doping, such as N-doping, is also an effective surface modification method. Nitrogen functional groups can promote the adsorption of aromatic VOCs, such as benzene and toluene by increasing the surface polarity [5,30]. Yang et al. [31] obtained porous carbon with a record-high acetone adsorption capacity after the N-doping modification of banana peel-derived activated carbon with urea. Different from conventional physical mixing, we achieved N-doping in the hydrothermal process and produced porous carbon with ultra-high porosity and excellent toluene adsorption capacity by subsequent KOH activation [32]. In our previous study, orange peel-derived porous carbon exhibited good VOCs adsorption effect. However, for raw materials of different compositions, the applicability of this method and the

VOCs adsorption performance of derived porous carbon requires further research.

In view of the above, this study aims to investigate the role of typical components in pore development and the VOCs adsorption performance of porous carbon from urea-assisted HTC and KOH activation. First, the effects of typical components on the physicochemical properties of porous carbon were investigated by using model compounds and orange peel added with components. Second, the chemical properties of the hydrochar were characterized to further reveal the influence of the components on porosity development. Finally, porous carbon was prepared from practical orange peels to verify the effect of typical components, which was further applied to quantify the VOCs adsorption performance.

2 Materials and methods

2.1 Materials

Five kinds of orange peels with different compositions were collected from a supermarket in Hubei province, where OP, OP1, OP2, OP3, and OP4 represented orange peel 0, orange peel 1, orange peel 2, orange peel 3, and orange peel 4, respectively. After drying in an oven at 105 °C for 24 h, they were ground into powder and sifted through a 200 µm sieve for later use. The industrial and elemental analyses of orange peels were carried out, and the chemical characteristics obtained were shown in Table 1. Except for OP, the industrial analysis and elemental composition of the other four kinds of orange peels showed little difference, all within 3 wt %. Therefore, these four kinds of orange peels were used as feedstock to compare the effect of composition, reducing the influence of chemical characteristics.

As the typical components of orange peel, cellulose (CAS 9004-34-6, Shanghai Aladdin Biochemical Technology Co., Ltd.), hemicellulose (CAS 9014-63-5, Shanghai Dibai Biotechnology Co., Ltd.), and lignin (CAS 9005-53-2, TCI (Shanghai) Chemical Industry Development Co., Ltd.) were purchased. KOH and urea were purchased from Sinopharm Chemical Reagent Co. Ltd., Shanghai. All reagents were used without further purification.

Table 1 Chemical characteristics of orange peels on dry basis

| Feedstock | Proximate analysis | | | Ultimate analysis | | | |
|-----------|------------------------|------------|---------------------|-------------------|-------------------------|----------|----------|
| | Volatile matter/(wt %) | Ash/(wt %) | Fixed carbon/(wt %) | C/(wt %) | O ^{a)} /(wt %) | H/(wt %) | N/(wt %) |
| OP | 75.13 | 1.57 | 23.30 | 48.96 | 42.03 | 5.34 | 1.09 |
| OP1 | 73.30 | 3.84 | 18.31 | 42.78 | 45.06 | 5.71 | 1.55 |
| OP2 | 72.43 | 3.77 | 18.18 | 42.68 | 45.89 | 5.49 | 1.08 |
| OP3 | 73.68 | 3.31 | 18.67 | 42.12 | 46.74 | 5.82 | 0.97 |
| OP4 | 73.17 | 2.94 | 19.38 | 44.29 | 44.30 | 5.77 | 1.65 |

a) By difference.

2.2 Preparation of N-doped hydrochar and derived porous carbons

Typical components were hydrothermally carbonized and KOH activated to preliminarily investigate their effects (Fig. 1). First, 15 g model compounds or OP was mixed with 120 mL of 10 wt % urea solution in a 250 mL stainless steel reactor. The hydrothermal process was performed at 210 °C for 2 h under autogenic pressure in an argon atmosphere with 200 r·min⁻¹ magnetic flux speed. The solid products were separated by vacuum filtration and cleaned with sufficient deionized water. After drying at 80 °C for 12 h, the hydrochar derived from each component (cellulose, hemicellulose, and lignin) and OP was named X-char, where X represented the feedstock. Then the dried N-doped hydrochar and KOH were mixed and ground in a mortar with a mass ratio of 1:2 (hydrochar/KOH), then the mixture was activated at 800 °C for 2 h at a heating rate of 3 °C·min⁻¹ in a horizontal tubular furnace in a nitrogen atmosphere. After cooling to room temperature, the samples were washed several times with sufficient 10 wt % hydrochloric acid and deionized water until neutral pH to remove KOH and residual products. The obtained porous carbon was dried at 105 °C for 12 h and named X-PC, where X represented the feedstock.

Orange peel added with typical components was used to further clarify the influence of components on the physicochemical properties and pore development of the porous carbon. The compositions of the raw materials were adjusted by adding 10 g model compounds (cellulose, hemicellulose, and lignin) to 5 g OP. The hydrochar and porous carbon were denoted as OP-X-char and OP-X-PC, with X representing the

typical components of orange peel (cellulose, hemicellulose, and lignin).

With similar physical structures but different chemical compositions, four kinds of orange peels were selected as the raw materials. They were hydrothermally treated and activated to verify the effect of typical components and explore the influence of composition on the toluene adsorption performance of porous carbon. The feedstock went through the same hydrothermal treatment and activation process as the above orange peels. The N-doped hydrochar was obtained and denoted as OPx-char, and the porous carbon was named OPx-PC, with x representing the orange peel species.

2.3 Characterization and analytical methods

To study the pore structure of porous carbons, nitrogen adsorption–desorption isotherms were measured by gas sorption analyzer (Quantachrome, Autosorb IQ, USA) at the liquid nitrogen temperature (77 K). The specific surface area was calculated by the Brunauer–Emmett–Teller (BET) method, and the specific surface area of micropores was obtained by the t-plot method. The pore size distribution characteristics were analyzed by quench solid density functional theory. To reveal the surface morphology, scanning electron microscope (SEM) images of the porous carbon were acquired on a field emission SEM (FE-SEM, ZEISS, Gemini Sigma 300, Germany, 2 keV). The elemental compositions of the samples were determined using an elemental analyzer (Vario Micro cube, Germany) for CHNS. To investigate the chemical properties of the hydrochar, surface element distributions were analyzed using X-ray photoelectron spectroscopy (XPS, Kratos, AXIS-ULTRA DLD-600W).

| Raw materials | Short names | | Hydrochar | Porous carbons |
|-------------------------------|--------------------|------------------------|--------------|----------------|
| Orange peel 0 | OP 15 g | | OP-char | OP-PC |
| Cellulose | Cel 15 g | 10 wt% urea solution | Cel-char | Cel-PC |
| Hemicellulose | Hcel 15 g | | Hcel-char | Hcel-PC |
| Lignin | Lig 15 g | | Lig-char | Lig-PC |
| Orange peel 0 + cellulose | OP 10 g + Cel 5 g | 210 °C, 2 h | OP-Cel-char | OP-Cel-PC |
| Orange peel 0 + hemicellulose | OP 10 g + Hcel 5 g | | OP-Hcel-char | OP-Hcel-PC |
| Orange peel 0 + lignin | OP 10 g + Lig 5 g | | OP-Lig-char | OP-Lig-PC |
| Orange peel 1 | OP1 15 g | Hydrothermal treatment | OP1-char | OP1-PC |
| Orange peel 2 | OP2 15 g | | OP2-char | OP2-PC |
| Orange peel 3 | OP3 15 g | | OP3-char | OP3-PC |
| Orange peel 4 | OP4 15 g | | OP4-char | OP4-PC |

Fig. 1 Preparation method of hydrochar and porous carbons.

And XPS PEAK 41 software was used for the decomposition of XPS spectrums.

To evaluate the VOCs adsorption performance of porous carbon, a dynamic toluene adsorption test was conducted. The porous carbon was placed in a fixed bed reactor (4 mm inner diameter) combined with a gas chromatography (GC9790 II). The weight of the adsorbent was approximately 20 mg and the adsorption temperature was 30 °C, with nitrogen as the carrier gas to achieve a total flow rate of 100 mL·min⁻¹ with an appropriate toluene concentration of 600 ppm (10⁻⁶). Before adsorption, the porous carbon was outgassed in nitrogen at 150 °C for 1 h. The breakthrough curves for toluene were obtained by graphical representation, showing the outlet concentration of toluene versus the test time. The equilibrium dynamic adsorption capacity (Q , mg toluene·g⁻¹) was calculated by numerical integration of the breakthrough curves in the previous study (Eq. (1)) [33],

$$Q = \frac{FC_0M \left[t_a - \int_0^{t_a} (C_t/C_0)dt \right]}{m}. \quad (1)$$

In Eq. (1), C_0 and C_t are the toluene concentrations at the inlet and outlet of the reactor, respectively. F is the molar flow rate of the gas, m is the adsorbent weight, t_a is the equilibrium time, and M is the molar mass of toluene.

3 Results and discussion

3.1 Effect of typical components on physicochemical properties of porous carbons

The pore structure parameters of the porous carbon from OP and model compounds were shown (Table 2). Hcel-PC possessed the highest specific surface area (2934 m²·g⁻¹) and abundant micropores. The specific surface area of the porous carbon prepared from cellulose was the lowest (1643 m²·g⁻¹), indicating the worst effect. The porosity of Lig-PC was between those of Hcel-PC and Cel-PC, while the microporous structure was abundant. Therefore, for urea-assisted HTC and KOH activation of typical components, hemicellulose was the most suitable for preparing porous carbon with high porosity, followed by lignin, and cellulose was the most unfavorable.

The surface morphology of the porous carbon derived

from orange peels with different compositions was shown in Fig. 2. OP-PC showed abundant pore structure and a large number of mesopores on its surface in Fig. 2(a). However, OP-Cel-PC possessed a smoother surface and worse pore structure, as shown in Fig. 2(b). The mesoporous structure also decreased significantly compared with that of OP-PC, indicating that the increase of cellulose was not conducive to pore development. With a denser surface than OP-PC, the pore density of OP-Hcel-PC increased obviously (Fig. 2(c)). OP-Lig-PC also showed a flatter and smoother surface in Fig. 2(d) than OP-PC, which may be caused by smaller pores. However, more detailed pore changes need to be determined further.

Figure 3 showed the detailed pore structure of the porous carbon measured by the gas sorption analyzer. The N₂ adsorption-desorption isotherms and the specific surface area of the porous carbon were compared in Figs. 3(a) and 3(b). With the addition of hemicellulose, the specific surface area and pore volume of OP-Hcel-PC were significantly higher than those of OP-PC. The total specific surface area increased by 231 m²·g⁻¹. The specific surface area of micropores increased by 510 m²·g⁻¹, whereas the specific surface area of mesopores decreased. In other words, hemicellulose promoted pore formation, especially the micropore formation in porous carbon. Compared with OP-PC, the specific surface area of OP-Cel-PC decreased dramatically by 494 m²·g⁻¹, primarily due to the reduction of mesopores. When lignin was added, the total porosity of OP-Lig-PC slightly decreased. The specific surface area of micropores increased by 512 m²·g⁻¹, whereas mesopore structure was significantly reduced. In general, hemicellulose was beneficial to pore structure development, particularly micropores. But cellulose was adverse to pore formation during urea-assisted HTC and activation. Lignin resulted in slightly worse total porosity and better microporosity of the porous carbon.

Regarding the pore size distribution in Figs. 3(c) and 3(d), the colored area represented the relative change of the pore amount in the corresponding pore size range. Compared with OP-PC, OP-Hcel-PC possessed richer pores in the range of 0.75–0.9 nm. Besides, the pores in the range of 1.0–1.4 and 1.85–2.9 nm increased slightly. As micropores provide principal adsorption sites for VOCs adsorption, the increased micropores can effectively improve the VOCs adsorption capacity [34,35]. However, the pore structure of 2.9–8.0 nm was

Table 2 Pore structure parameters of porous carbon from OP and model compounds

| Sample | $S_{\text{BET}}/(\text{m}^2 \cdot \text{g}^{-1})$ | $S_{\text{micro}}^{\text{a})}/(\text{m}^2 \cdot \text{g}^{-1})$ | $S_{\text{meso}}^{\text{b})}/(\text{m}^2 \cdot \text{g}^{-1})$ | Pore volume/(cm ³ ·g ⁻¹) | $V_{\text{micro}}^{\text{c})}/(\text{cm}^3 \cdot \text{g}^{-1})$ | $V_{\text{meso}}^{\text{d})}/(\text{cm}^3 \cdot \text{g}^{-1})$ |
|---------|---|---|--|---|--|---|
| OP-PC | 2651 | 1752 | 899 | 1.46 | 0.78 | 0.68 |
| Cel-PC | 1643 | 1388 | 255 | 0.87 | 0.59 | 0.28 |
| Hcel-PC | 2934 | 2253 | 681 | 1.51 | 1.00 | 0.51 |
| Lig-PC | 2363 | 2140 | 223 | 1.05 | 0.88 | 0.17 |

a) S_{micro} : the specific surface area of micropore; b) S_{meso} : the specific surface area of mesopore; c) V_{micro} : the pore volume of micropore; d) V_{meso} : the pore volume of mesopore.

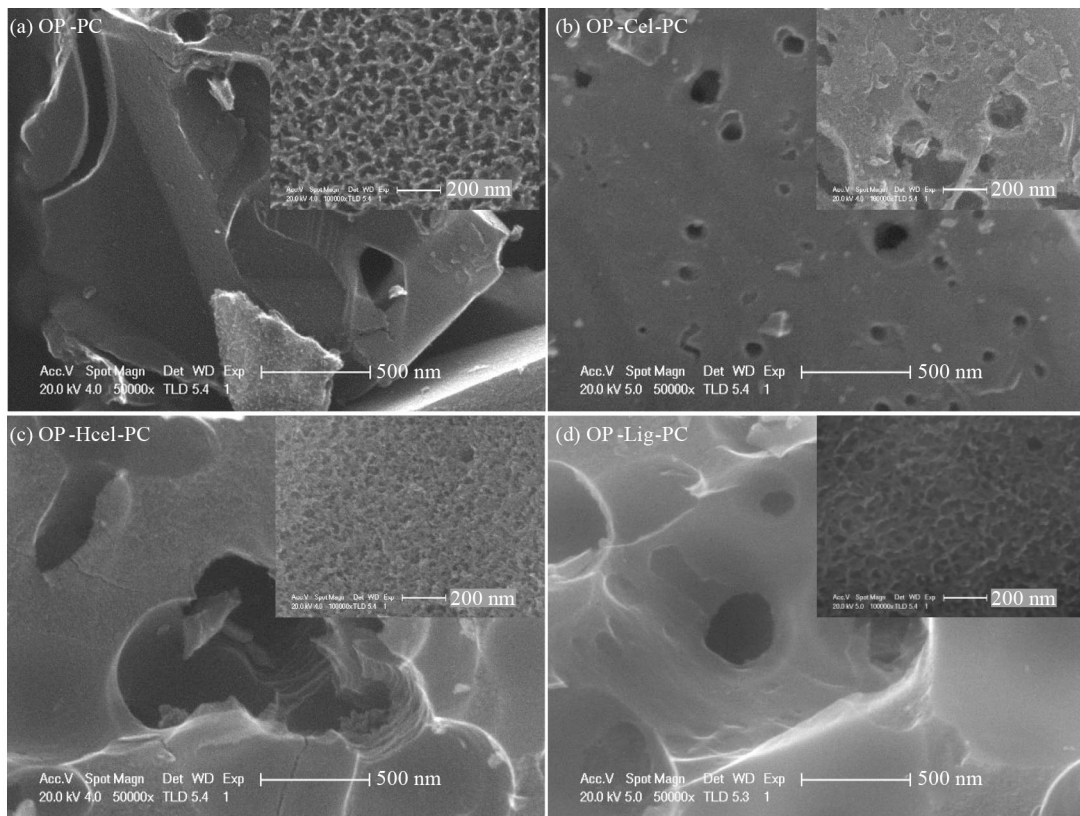


Fig. 2 SEM images of porous carbon from orange peels with different compositions: (a) OP-PC, (b) OP-Cel-PC, (c) OP-Hcel-PC, and (d) OP-Lig-PC.

reduced, which hindered the rapid capture of toluene and prolonged the adsorption time [34,36]. These results explained the addition of hemicellulose significantly increased the specific surface area of micropores and decreased the specific surface area of mesopores. As for OP-Cel-PC, the pores in the range of 0.72–0.84 and 2–2.65 nm became more abundant, while the pore structure declined at 0.84–1.05, 1.1–2.0, and 2.65–10 nm. Therefore, the specific surface area of mesopores in OP-Cel-PC was significantly reduced. There were more micropores in OP-Lig-PC than in OP-PC in the 0.5–0.55, 0.72–0.85, and 1–1.2 nm ranges. The narrower micropores (size < 0.7 nm) can better reflect benzene adsorption capacity [37]. For VOCs of small molecules, narrow micropores are more conducive to improving the adsorption capacity. Although the micropores of 0.85–1 and 1.2–1.96 nm declined, the total specific surface area of micropores of OP-Lig-PC increased. In addition, the pore structure of 2–2.7 nm increased, while the pores in 2.7–10 nm considerably decreased, resulting in an apparent reduction of mesopores. To sum up, hemicellulose was the major contributor to the porosity and micropore development of porous carbon, which was beneficial to improving the VOCs adsorption performance. Cellulose caused both the micropore and mesopore structure of porous carbon worse, indicating it was unfavorable for pore development, while lignin led to richer micropores and poorer mesopores.

The ultimate analysis of the porous carbon prepared from OP with typical components added was shown in Table 3. Although the contents of the typical components in the feedstock were different, the ultimate porous carbon varied little in the elemental composition. The difference in C and O content was within 2 wt %. The nitrogen of porous carbon was almost absent, and the difference was even smaller (less than 0.4 wt %). These results indicated that with the addition of typical components, the chemical properties of porous carbon changed little, which hardly affected the VOCs adsorption performance.

The effect of the typical components for orange peel on the physicochemical properties of porous carbon was clarified. The addition of different components had minimal effect on the chemical properties of the derived porous carbon. While the pore structure varied, the VOCs adsorption performance changed significantly. That is, the typical components contributed differently to the pore development, which was influenced by the physicochemical properties of the precursors. To reveal the influence mechanism, it was necessary to study the chemical properties of the hydrochar.

3.2 Influence of typical components on chemical properties of hydrochar

The ultimate analysis of the hydrochar was given in

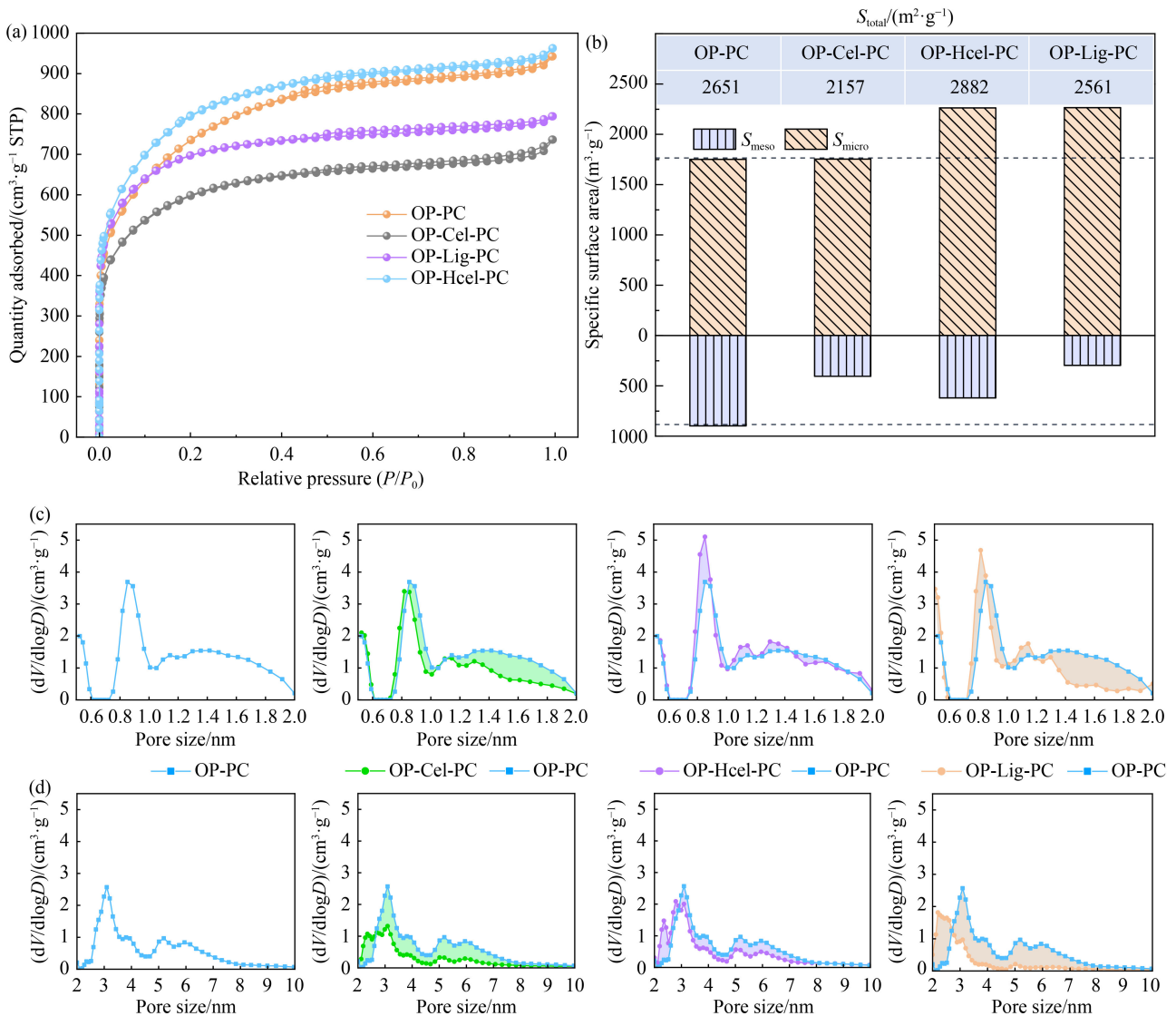


Fig. 3 (a) N₂ adsorption–desorption isotherms; (b) the specific surface area; (c) micropore distribution; (d) mesopore distribution of porous carbon from OP with typical components added.

Table 3 Ultimate analysis of porous carbon from OP with typical components added

| Sample | C/(wt %) | O ^{a)} /(wt %) | H/(wt %) | N/(wt %) |
|------------|----------|-------------------------|----------|----------|
| OP-PC | 87.48 | 10.73 | 0.91 | 0.77 |
| OP-Cel-PC | 88.33 | 10.18 | 0.88 | 0.53 |
| OP-Hcel-PC | 88.19 | 10.12 | 0.87 | 0.75 |
| OP-Lig-PC | 89.32 | 9.32 | 0.92 | 0.40 |

a) By difference.

Table 4. Comparing the hydrochar prepared from individual components, Hcel-char possessed lower H/C and O/C ratios, indicating more severe dehydration and decarboxylation. In addition, it was noteworthy that with the highest N content of 14.73 wt % and the lowest O content, Hcel-char produced porous carbon with the highest porosity. Cel-char showed the opposite results: the lowest N content, the highest O content, and the worst pore structure of the derived porous carbon. As for

OP-char, the N content reached 6.55 wt % after urea-assisted HTC. Compared with OP-char, OP-Hcel-char was obtained by undergoing more intense dehydration and decarboxylation, and the N content increased significantly to 9.8 wt %. The changes of OP-Cel-char were contrary when the content of cellulose increased. The addition of lignin significantly decreased the O/C ratios, illustrating intensified dehydration reaction, while the N content of OP-Lig-char decreased slightly. The different degrees of hydrothermal reactions were related to the urea-assisted hydrothermal environment. Urea decomposed into ammonia water and CO₂ in the hydrothermal process [38], which was verified by the residual hydrothermal liquid turning the red litmus paper turn blue (Fig. 4). In the ammonia environment, the hydrolysis degree of lignin was the highest, followed by hemicellulose, which was conducive to subsequent dehydration and decarboxylation, the hydrolysis degree of cellulose was the

lowest [39,40]. In summary, through different degrees of hydrothermal reactions, the oxygen and nitrogen contents of hydrochar varied significantly, which played an essential role in the KOH activation process.

To further study the evolution of OFGs, XPS was carried out on different hydrochar. The XPS C 1s spectrum of the hydrochar contained four peak spectra: aliphatic/aromatic carbon groups (CH_x , $\text{C}-\text{C/C=C}$) (284.6 eV), hydroxyl/amino groups ($-\text{C}-\text{O}/-\text{C}-\text{N}$) (285.8 eV), carbonyl/imine groups ($>\text{C=O}/>\text{C=N}$) (287.3 eV) and carboxylic groups, esters or lactones ($-\text{COOR}$) (289.0 eV)

Table 4 Ultimate analysis of hydrochar on dry basis*

| Sample | C/(wt %) | O ^a /(wt %) | H/(wt %) | N/(wt %) | O/C ^b | H/C ^b | N/C ^b |
|--------------|----------|------------------------|----------|----------|------------------|------------------|------------------|
| Cel-char | 44.53 | 48.08 | 6.20 | 1.19 | 0.81 | 1.67 | 0.02 |
| Heel-char | 61.38 | 18.67 | 5.22 | 14.73 | 0.23 | 1.02 | 0.21 |
| Lig-char | 62.23 | 29.87 | 5.03 | 2.87 | 0.36 | 0.97 | 0.04 |
| OP-char | 54.76 | 32.88 | 5.81 | 6.55 | 0.45 | 1.27 | 0.10 |
| OP-Cel-char | 51.50 | 37.36 | 5.86 | 5.28 | 0.54 | 1.37 | 0.09 |
| OP-Heel-char | 57.38 | 27.37 | 5.46 | 9.80 | 0.36 | 1.14 | 0.15 |
| OP-Lig-char | 57.61 | 31.54 | 5.30 | 5.55 | 0.41 | 1.10 | 0.08 |

* Lower Linear range Higher

a) By difference; b) atomic ratio.

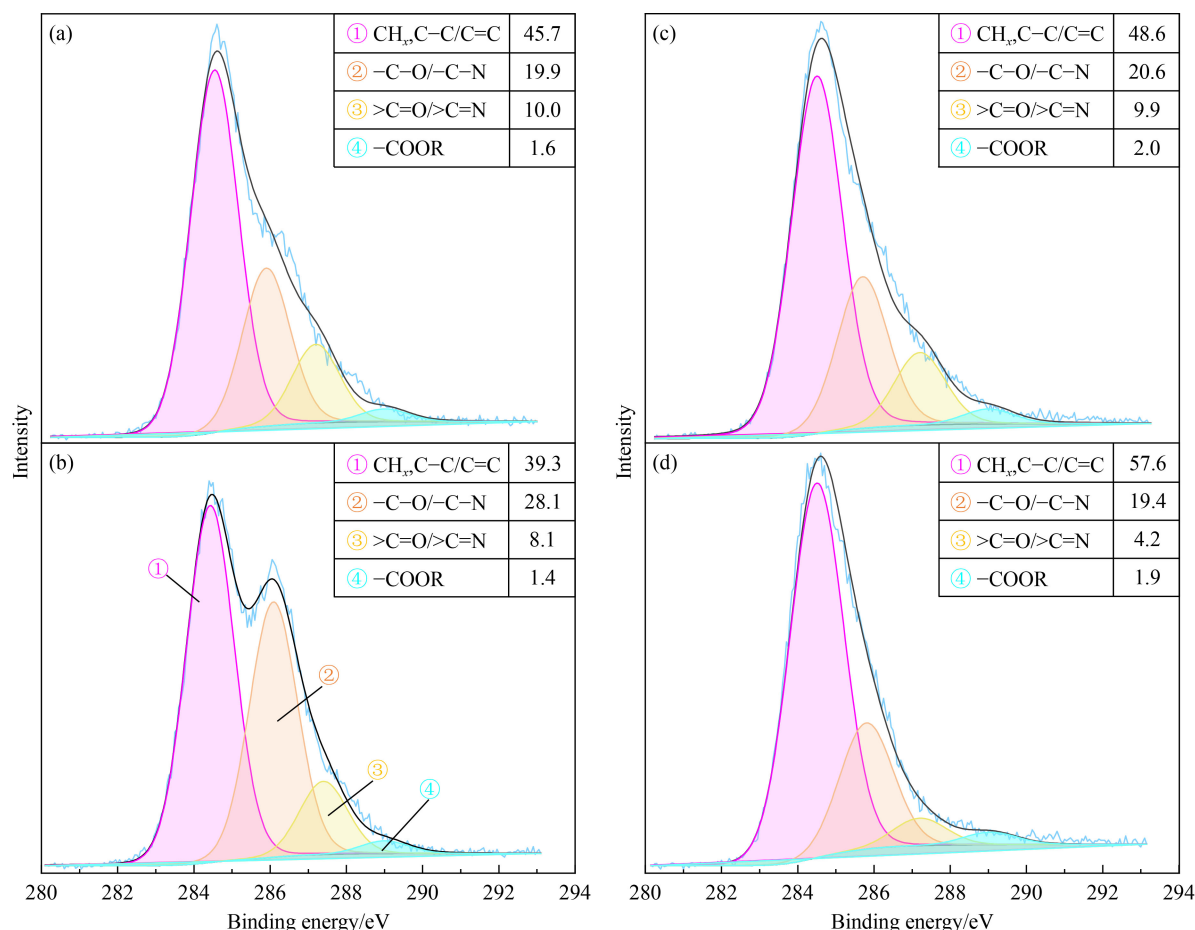


Fig. 5 XPS C 1s spectra and atomic relative contents (wt %) of different carbon in (a) OP-char, (b) OP-Cel-char, (c) OP-Heel-char, and (d) OP-Lig-char.

[23,41,42]. The normalized peak intensities of the carbon functionalities were listed in Fig. 5. Compared with OP-char, OP-Heel-char possessed more $-\text{COOR}$ functional groups containing esters and lactones, which helped improve the chemical activation potential. As for the increase of $-\text{C}-\text{O}/-\text{C}-\text{N}$, it could be inferred that this was related to richer amino groups based on the abundant

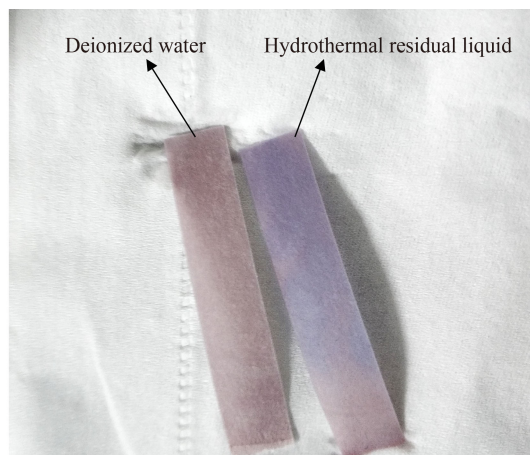


Fig. 4 Litmus test.

nitrogen in OP-Hcel-char. OP-Cel-char possessed the lowest C content and the highest O content. Significantly decreased $>\text{C=O}/>\text{C=N}$ content and increased $-\text{C-O}/-\text{C-N}$ content were mainly due to the reduction of carbonyl groups and the rise of hydroxyl groups caused by weaker hydrothermal reactions. For OP-Lig-char, the significant decrease in $>\text{C=O}/>\text{C=N}$ meant carbonyl groups declined predominantly, and the increment of $-\text{COOR}$ represented ester and carboxyl groups increased.

To clarify the distribution of surface nitrogen structures, the N 1s spectra of hydrochar were shown in Fig. 6. After peak correction, four N 1s signals were identified at 398.3 ± 0.1 , 399.1 ± 0.1 , 400.2 ± 0.1 , and 401.4 ± 0.1 eV, which were attributed to the pyridinic-N, amine-N, pyrrolic/pyridonic-N, and graphitic-N, respectively [43–45]. For OP-char, the nitrogen mainly consisted of amine-N, pyrrolic/pyridonic-N, and pyridinic-N. These nitrogen functional groups were introduced into the hydrochar mainly by the reactions of intermediates such as furfural, furan with urea or amines in the hydrothermal process [46–48]. These nitrogen structures can facilitate pore formation by reacting with activating agents during activation [32].

Hemicellulose improved the four nitrogen structures to different degrees, which may be related to forming more intermediates that can react with amines owing to stronger reactions. In particular, the amine-N and pyrrolic/pyridonic-N content of OP-Hcel-char significantly increased, which could effectively promote pore development during KOH activation. In contrast, cellulose reduced the amine-N and pyrrolic/pyridonic-N of the hydrochar. Although the total nitrogen of OP-Lig-char declined, the pyrrolic/pyridonic-N and graphitic-N contents increased slightly, which improved the porosity by participating in reactions during activation.

According to the above, the influence of the typical components on the porosity development of porous carbon can be inferred. Hemicellulose maintained a high degree of hydrolysis during the urea-assisted hydrothermal process, which was conducive to subsequent dehydration and decarboxylation. These resulted in increased OFGs, including esters and lactones. Besides, stronger hydrothermal reactions produced more intermediates containing furfural, which could react with amines or urea, such as the Maillard reaction between carbonyl groups and amines [49,50]. Then the abundant nitrogen

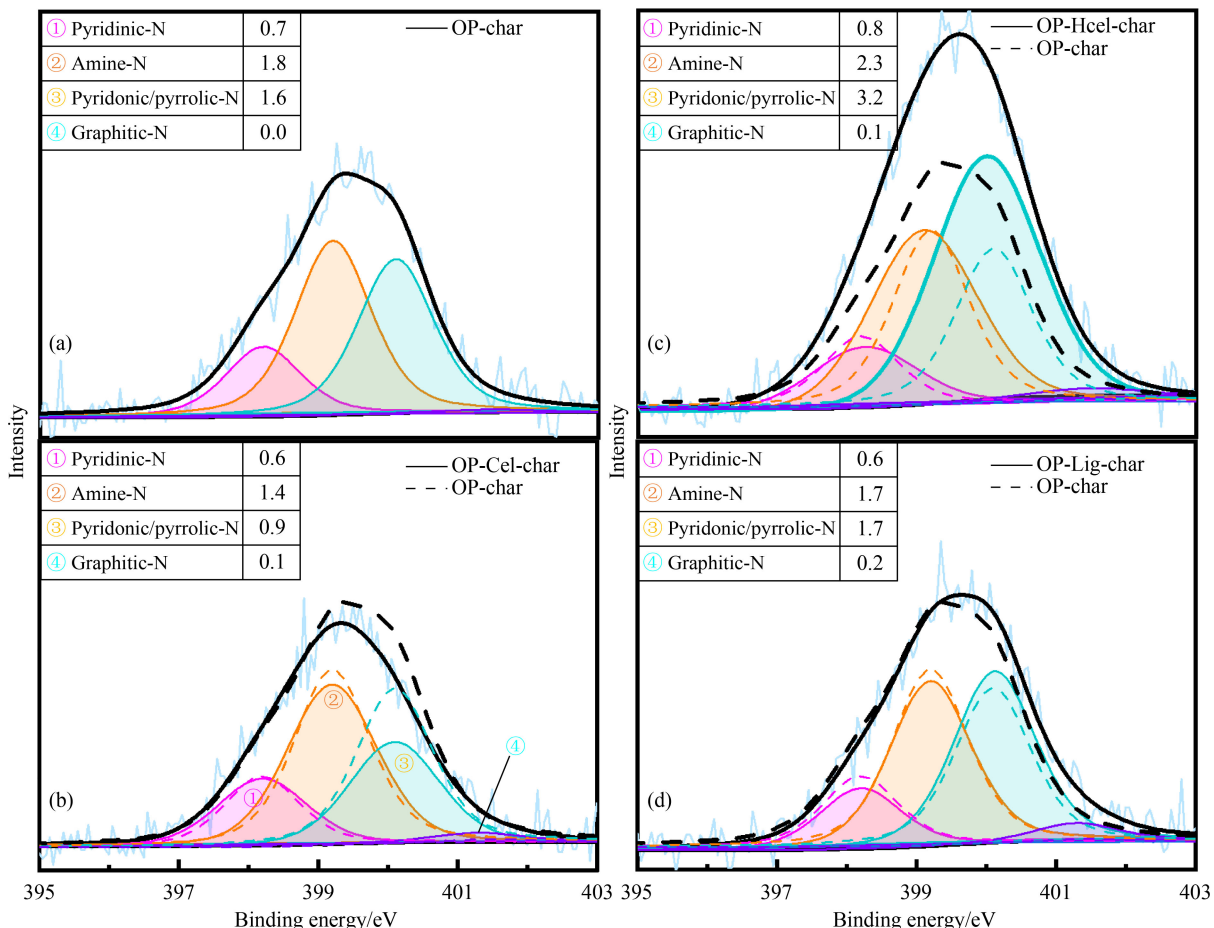


Fig. 6 XPS N 1s spectra and atomic relative contents (wt %) of different nitrogen in (a) OP-char, (b) OP-Cel-char, (c) OP-Hcel-char, and (d) OP-Lig-char.

functional groups, especially amine-N and pyrrolic/pyridonic-N, were successfully incorporated into the hydrochar. Therefore, hemicellulose improved the OFGs content and N-doping effect, which further enhanced the porosity and microporosity of the porous carbon. The enhancement of microporous structure can effectively improve the VOCs adsorption capacity. However, the weaker hydrothermal reactions of cellulose resulted in significantly increased hydroxyl groups and slightly decreased carbonyl groups. And intermediates containing carbonyl groups also declined, which was unfavorable to reactions with amines and led to a significant reduction in N content. Cellulose generally increased the OFGs of hydrochar, but decreased the nitrogen, especially amine-N and pyrrolic/pyridonic-N, which deteriorated the porosity of porous carbon. The hydrothermal reaction of lignin was still severe under urea-assisted hydrothermal treatment, and the intermediates were mainly phenols that could hardly react with amines or urea [27]. This could explain the slightly decreased nitrogen and significantly reduced carbonyl groups in the hydrochar, which led to slightly worse

porosity. However, the increase of pyrrolic/pyridonic-N and graphitic-N was conducive to pore development, which may be responsible for the improvement in micropores and contribute to small molecule VOCs adsorption.

3.3 Toluene adsorption performance of porous carbon

The toluene adsorption capacity and pore structure of porous carbon prepared from four kinds of orange peels were measured (Fig. 7). Toluene adsorption tests were carried out on the porous carbon. Adsorption breakthrough curves and adsorption capacity for toluene were shown in Figs. 7(a) and 7(b), respectively. The obtained porous carbon all possessed good toluene adsorption performance, and the adsorption capacity significantly increased from $382.8 \text{ mg}\cdot\text{g}^{-1}$ for OP1-PC to $485.3 \text{ mg}\cdot\text{g}^{-1}$ for OP4-PC. The difference in the toluene adsorption capacity of the derived porous carbon reached 26.8% for the four kinds of orange peels with similar physical structures. The elemental analysis in Table 5

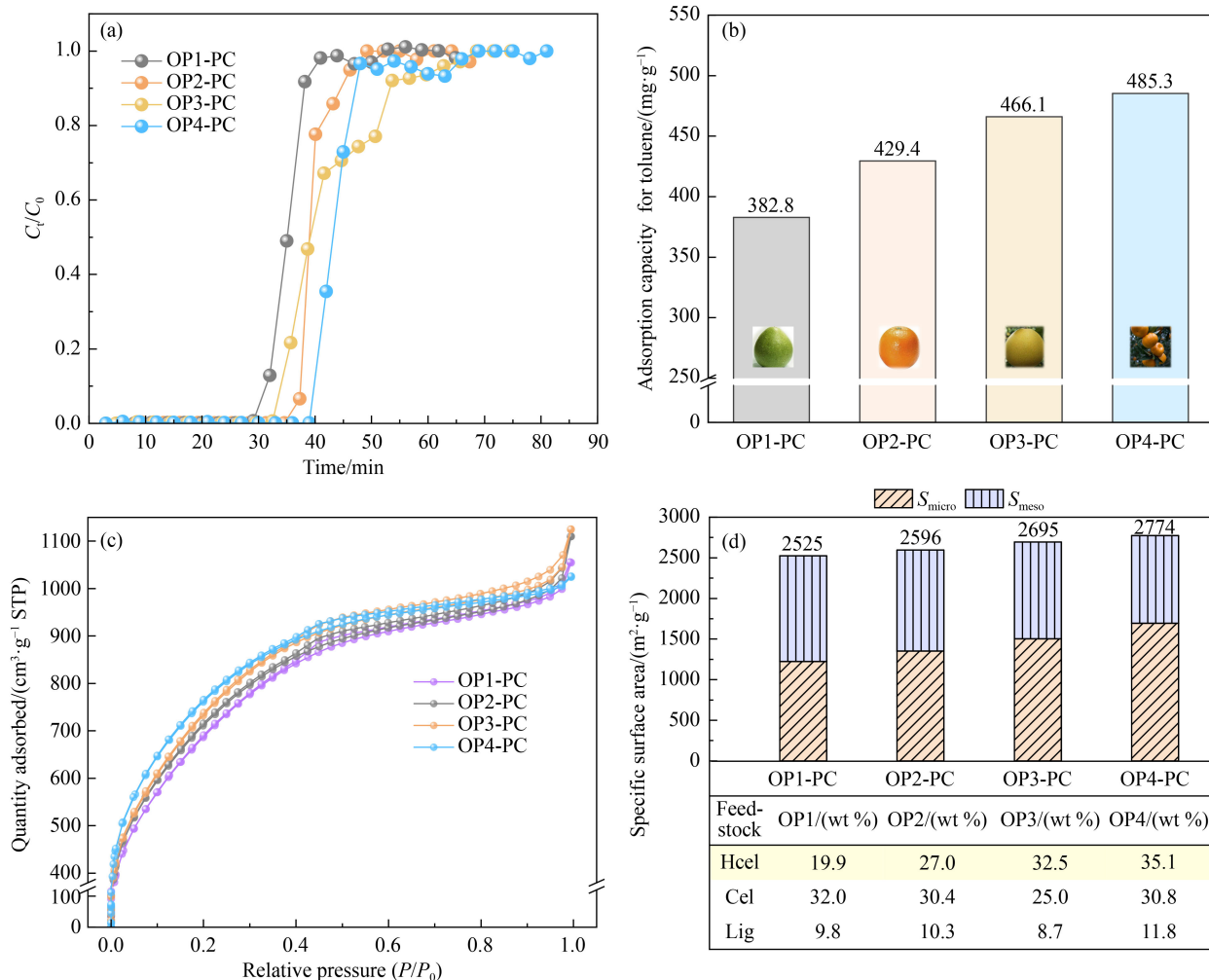


Fig. 7 (a) Adsorption breakthrough curves; (b) adsorption capacity of porous carbon for toluene; (c) N_2 adsorption–desorption isotherms; (d) the contents of three components (wt %) for orange peel and the specific surface area of derived porous carbons.

Table 5 Ultimate analysis of hydrochar and porous carbon on dry basis

| Sample | C/(wt %) | O ^a /(wt %) | H/(wt %) | N/(wt %) |
|----------|----------|------------------------|----------|----------|
| OP1-char | 49.24 | 40.06 | 5.03 | 5.61 |
| OP2-char | 50.52 | 37.88 | 5.18 | 6.37 |
| OP3-char | 50.99 | 36.15 | 5.35 | 7.47 |
| OP4-char | 50.98 | 37.38 | 5.51 | 6.08 |
| OP1-PC | 69.09 | 27.49 | 1.55 | 1.54 |
| OP2-PC | 69.06 | 26.98 | 1.49 | 2.04 |
| OP3-PC | 69.93 | 26.79 | 1.33 | 1.69 |
| OP4-PC | 76.34 | 20.46 | 1.40 | 1.51 |

a) By difference.

showed that the porous carbon had fairly low nitrogen content (less than 2 wt %), indicating that surface nitrogen functional groups were not the cause of the difference in adsorption performance. The N₂ adsorption–desorption isotherms of porous carbon were measured, and their specific surface area was calculated (Figs. 7(c) and 7(d)). The results showed that the porous carbon from four kinds of orange peels all had the specific area of more than 2500 m²·g⁻¹ despite the variable compositions, demonstrating the effectiveness of the urea-assisted HTC and KOH activation method. This was because the rich nitrogen of hydrochar was conducive to pore expansion during activation, which can also be proved by Table 5. The specific surface area increased from 2525 m²·g⁻¹ for OP1-PC to 2774 m²·g⁻¹ for OP4-PC, and the specific surface area of micropores increased continuously, which could explain the better toluene adsorption performance.

Since the physical structures of orange peels are similar, the effect of typical components can be further verified by HTC and activation of practical orange peels. As the main components of orange peel are lignin, cellulose, and hemicellulose, and their contents were further determined by the methods in the literature [51–53] (Fig. 7(d)). The contents of lignin and cellulose changed little in the orange peels, with the hemicellulose content increasing from 19.9 wt % for OP1 to 35.1 wt % for OP4. The specific surface area of derived porous carbon increased, and the micropore structure was obviously richer. Even though the cellulose and lignin content varied little, the specific surface area of porous carbon was positively correlated with the hemicellulose content ($R^2 = 0.953$, $P = 0.023$). These results verified that hemicellulose effectively increased the total porosity and microporosity of porous carbon during urea-assisted HTC and KOH activation, which further promoted the toluene adsorption capacity.

4 Conclusions

The role of hemicellulose, cellulose, and lignin in the porosity development and the toluene adsorption performance of porous carbon during urea-assisted HTC

and KOH activation was investigated in this study. Hemicellulose was the major contributor to the porosity and microporosity of porous carbon due to the richer amine-N, pyrrolic/pyridonic-N, and COOR of hydrochar. These changes can promote porosity, especially micropore formation during the activation process. The toluene adsorption capacity was significantly increased from 382.8 to 485.3 mg·g⁻¹ with the increase of hemicellulose content in orange peel. Cellulose bestowed hydrochar with reduced amine-N, pyrrolic/pyridonic-N, and >C=O, which deteriorated the porosity and adversely affected the toluene adsorption. Lignin slightly increased –COOR, pyrrolic/pyridonic-N, and graphitic-N and decreased >C=O in the hydrochar, resulting in comparatively worse porosity and more abundant micropores. The obtained porous carbon possessed abundant micropores and high specific area, with the highest up to 2882 m²·g⁻¹. This study can promote the high-value utilization of biomass waste and provide a reference for selecting suitable feedstock to synthesize porous carbon with better porosity for effective VOCs removal.

Acknowledgements This work was supported by the Shenzhen Science and Technology Program (Grant No. JSGG20210802154804013). The authors also thank the Analytical and Testing Center of Huazhong University of Science and Technology for testing of the samples.

References

1. Gałżowska G, Chraniuk M, Wolska L. *In vitro* assays as a tool for determination of VOCs toxic effect on respiratory system: a critical review. *Trends in Analytical Chemistry*, 2016, 77: 14–22
2. Zheng C, Shen J, Zhang Y, Huang W, Zhu X, Wu X, Chen L, Gao X, Cen K. Quantitative assessment of industrial VOC emissions in China: historical trend, spatial distribution, uncertainties, and projection. *Atmospheric Environment*, 2017, 150: 116–125
3. Colman Lerner J E, Sanchez E Y, Sambeth J E, Porta A A. Characterization and health risk assessment of VOCs in occupational environments in Buenos Aires, Argentina. *Atmospheric Environment*, 2012, 55: 440–447
4. Zhang Z, Jiang Z, Shangguan W. Low-temperature catalysis for VOCs removal in technology and application: a state-of-the-art review. *Catalysis Today*, 2016, 264: 270–278
5. Yang C, Miao G, Pi Y, Xia Q, Wu J, Li Z, Xiao J. Abatement of various types of VOCs by adsorption/catalytic oxidation: a review. *Chemical Engineering Journal*, 2019, 370: 1128–1153
6. Li X, Zhang L, Yang Z, Wang P, Yan Y, Ran J. Adsorption materials for volatile organic compounds (VOCs) and the key factors for VOCs adsorption process: a review. *Separation and Purification Technology*, 2020, 235: 116213
7. Twumasi E, Forslund M, Norberg P, Sjöström C. Carbon-silica composites prepared by the precipitation method. Effect of the synthesis parameters on textural characteristics and toluene

- dynamic adsorption. *Journal of Porous Materials*, 2012, 19(3): 333–343
- 8. Son H K, Sivakumar S, Rood M J, Kim B J. Electrothermal adsorption and desorption of volatile organic compounds on activated carbon fiber cloth. *Journal of Hazardous Materials*, 2016, 301: 27–34
 - 9. Jothi Ramalingam R, Sivachidambaram M, Vijaya J J, Al-Lohedan H A, Muthumareeswaran M R. Synthesis of porous activated carbon powder formation from fruit peel and cow dung waste for modified electrode fabrication and application. *Biomass and Bioenergy*, 2020, 142: 105800
 - 10. Jain A, Balasubramanian R, Srinivasan M P. Tuning hydrochar properties for enhanced mesopore development in activated carbon by hydrothermal carbonization. *Microporous and Mesoporous Materials*, 2015, 203: 178–185
 - 11. Singh G, Lakhi K S, Sil S, Bhosale S V, Kim I, Albahily K, Vinu A. Biomass derived porous carbon for CO₂ capture. *Carbon*, 2019, 148: 164–186
 - 12. Yin J, Zhang W, Alhebshi N A, Salah N, Alshareef H N. Synthesis strategies of porous carbon for supercapacitor applications. *Small Methods*, 2020, 4(3): 1900853
 - 13. Song M, Zhou Y, Ren X, Wan J, Du Y, Wu G, Ma F. Biowaste-based porous carbon for supercapacitor: the influence of preparation processes on structure and performance. *Journal of Colloid and Interface Science*, 2019, 535: 276–286
 - 14. Zhao P, Shen Y, Ge S, Chen Z, Yoshikawa K. Clean solid biofuel production from high moisture content waste biomass employing hydrothermal treatment. *Applied Energy*, 2014, 131: 345–367
 - 15. Shen Y, Zhang N. A facile synthesis of nitrogen-doped porous carbons from lignocellulose and protein wastes for VOCs sorption. *Environmental Research*, 2020, 189: 109956
 - 16. Zhang X, Gao B, Fang J, Zou W, Dong L, Cao C, Zhang J, Li Y, Wang H. Chemically activated hydrochar as an effective adsorbent for volatile organic compounds (VOCs). *Chemosphere*, 2019, 218: 680–686
 - 17. Başakçılardan Kabakçı S, Baran S S. Hydrothermal carbonization of various lignocellulosics: fuel characteristics of hydrochars and surface characteristics of activated hydrochars. *Waste Management*, 2019, 100: 259–268
 - 18. Falco C, Baccile N, Titirici M. Morphological and structural differences between glucose, cellulose and lignocellulosic biomass derived hydrothermal carbons. *Green Chemistry*, 2011, 13(11): 3273
 - 19. Jain A, Balasubramanian R, Srinivasan M P. Hydrothermal conversion of biomass waste to activated carbon with high porosity: a review. *Chemical Engineering Journal*, 2016, 283: 789–805
 - 20. Basso D, Patuzzi F, Castello D, Baratieri M, Rada E C, Weiss-Hortala E, Fiori L. Agro-industrial waste to solid biofuel through hydrothermal carbonization. *Waste Management*, 2016, 47: 114–121
 - 21. Libra J A, Ro K S, Kammann C, Funke A, Berge N D, Neubauer Y, Titirici M, Fühner C, Bens O, Kern J, Emmerich K-H. Hydrothermal carbonization of biomass residuals: a comparative review of the chemistry, processes and applications of wet and dry pyrolysis. *Biofuels*, 2011, 2(1): 71–106
 - 22. Ogihara Y, Smith R L, Inomata H, Arai K. Direct observation of cellulose dissolution in subcritical and supercritical water over a wide range of water densities (550–1000 kg·m⁻³). *Cellulose*, 2005, 12(6): 595–606
 - 23. Sevilla M, Fuertes A B. The production of carbon materials by hydrothermal carbonization of cellulose. *Carbon*, 2009, 47(9): 2281–2289
 - 24. Kang S, Li X, Fan J, Chang J. Characterization of hydrochars produced by hydrothermal carbonization of lignin, cellulose, D-xylose, and wood meal. *Industrial & Engineering Chemistry Research*, 2012, 51(26): 9023–9031
 - 25. Fang Z, Sato T, Smith R L, Inomata H, Arai K, Kozinski J A. Reaction chemistry and phase behavior of lignin in high-temperature and supercritical water. *Bioresource Technology*, 2008, 99(9): 3424–3430
 - 26. Dinjus E, Kruse A, Tröger N. Hydrothermal carbonization: 1. Influence of lignin in lignocelluloses. *Chemical Engineering & Technology*, 2011, 83(10): 1734–1741
 - 27. Xiao K, Liu H, Li Y, Yi L, Zhang X, Hu H, Yao H. Correlations between hydrochar properties and chemical constitution of orange peel waste during hydrothermal carbonization. *Bioresource Technology*, 2018, 265: 432–436
 - 28. Jain A, Balasubramanian R, Srinivasan M P. Production of high surface area mesoporous activated carbons from waste biomass using hydrogen peroxide-mediated hydrothermal treatment for adsorption applications. *Chemical Engineering Journal*, 2015, 273: 622–629
 - 29. Islam M A, Ahmed M J, Khanday W A, Asif M, Hameed B H. Mesoporous activated coconut shell-derived hydrochar prepared via hydrothermal carbonization-NaOH activation for methylene blue adsorption. *Journal of Environmental Management*, 2017, 203: 237–244
 - 30. Zhu M, Zhou K, Sun X, Zhao Z, Tong Z, Zhao Z. Hydrophobic N-doped porous biocarbon from dopamine for high selective adsorption of p-xylene under humid conditions. *Chemical Engineering Journal*, 2017, 317: 660–672
 - 31. Yang F, Li W, Zhang L, Tu W, Wang X, Li L, Yu C, Gao Q, Yuan A, Pan J. Drastically boosting volatile acetone capture enabled by N-doping activated carbon: an interesting deep surface digging effect. *Separation and Purification Technology*, 2021, 276: 119280
 - 32. Xiao K, Liu H, Li Y, Yang G, Wang Y, Yao H. Excellent performance of porous carbon from urea-assisted hydrochar of orange peel for toluene and iodine adsorption. *Chemical Engineering Journal*, 2020, 382: 122997
 - 33. Romero-Anaya A J, Lillo-Ródenas M A, Linares-Solano A. Activation of a spherical carbon for toluene adsorption at low concentration. *Carbon*, 2014, 77: 616–626
 - 34. Zhang X, Gao B, Creamer A E, Cao C, Li Y. Adsorption of VOCs onto engineered carbon materials: a review. *Journal of Hazardous Materials*, 2017, 338: 102–123
 - 35. Chen G, Yu H, Lin F, Zhang Z, Yan B, Song Y. Utilization of edible fungi residues towards synthesis of high-performance porous carbon for effective sorption of Cl-VOCs. *Science of the Total Environment*, 2020, 727: 138475
 - 36. Yang Y, Lin B, Sun C, Tang M, Lu S, Huang Q, Yan J. Facile

- synthesis of tailored mesopore-enriched hierarchical porous carbon from food waste for rapid removal of aromatic VOCs. *Science of the Total Environment*, 2021, 773: 145453
- 37. Lillo-Ródenas M A, Cazorla-Amorós D, Linares-Solano A. Behaviour of activated carbons with different pore size distributions and surface oxygen groups for benzene and toluene adsorption at low concentrations. *Carbon*, 2005, 43(8): 1758–1767
 - 38. Vasquez-Elizondo L J, Rendón-Ángeles J C, Matamoros-Veloz Z, López-Cuevas J, Yanagisawa K. Urea decomposition enhancing the hydrothermal synthesis of lithium iron phosphate powders: effect of the lithium precursor. *Advanced Powder Technology*, 2017, 28(6): 1593–1602
 - 39. Chen C, Boldor D, Aita G, Walker M. Ethanol production from sorghum by a microwave-assisted dilute ammonia pretreatment. *Bioresource Technology*, 2012, 110: 190–197
 - 40. Wang T, Zhai Y, Zhu Y, Li C, Zeng G. A review of the hydrothermal carbonization of biomass waste for hydrochar formation: process conditions, fundamentals, and physicochemical properties. *Renewable & Sustainable Energy Reviews*, 2018, 90: 223–247
 - 41. Si W, Zhou J, Zhang S, Li S, Xing W, Zhuo S. Tunable N-doped or dual N, S-doped activated hydrothermal carbons derived from human hair and glucose for supercapacitor applications. *Electrochimica Acta*, 2013, 107: 397–405
 - 42. Chen N, Huang Y, Hou X, Ai Z, Zhang L. Photochemistry of hydrochar: reactive oxygen species generation and sulfadimidine degradation. *Environmental Science & Technology*, 2017, 51(19): 11278–11287
 - 43. Wang D, Su D. Heterogeneous nanocarbon materials for oxygen reduction reaction. *Energy & Environmental Science*, 2014, 7(2): 576–591
 - 44. Rao L, Ma R, Liu S, Wang L, Wu Z, Yang J, Hu X. Nitrogen enriched porous carbons from *d*-glucose with excellent CO₂ capture performance. *Chemical Engineering Journal*, 2019, 362: 794–801
 - 45. Li Y, Zou B, Hu C, Cao M. Nitrogen-doped porous carbon nanofiber webs for efficient CO₂ capture and conversion. *Carbon*, 2016, 99: 79–89
 - 46. Wu Q, Li W, Liu S, Jin C. Hydrothermal synthesis of N-doped spherical carbon from carboxymethylcellulose for CO₂ capture. *Applied Surface Science*, 2016, 369: 101–107
 - 47. Seredych M, Hulicova-Jurcakova D, Lu G Q, Bandosz T J. Surface functional groups of carbons and the effects of their chemical character, density and accessibility to ions on electrochemical performance. *Carbon*, 2008, 46(11): 1475–1488
 - 48. Latham K G, Simone M I, Dose W M, Allen J A, Donne S W. Synchrotron based NEXAFS study on nitrogen doped hydrothermal carbon: insights into surface functionalities and formation mechanisms. *Carbon*, 2017, 114: 566–578
 - 49. Baccile N, Laurent G, Coelho C, Babonneau F, Zhao L, Titirici M. Structural insights on nitrogen-containing hydrothermal carbon using solid-state magic angle spinning ¹³C and ¹⁵N nuclear magnetic resonance. *Journal of Physical Chemistry C*, 2011, 115(18): 8976–8982
 - 50. Billaud C, Maraschin C, Chow Y, Chériot S, Peyrat-Maillard M, Nicolas J. Maillard reaction products as “natural antibrowning” agents in fruit and vegetable technology. *Molecular Nutrition & Food Research*, 2005, 49(7): 656–662
 - 51. Dominguez J M, Cao N, Gong C S, Tsao G T. Dilute acid hemicellulose hydrolysates from corn cobs for xylitol production by yeast. *Bioresource Technology*, 1997, 61(1): 85–90
 - 52. Kirk T K, Obst J R. Lignin determination. *Methods in Enzymology*, 1988, 161: 87–101
 - 53. Thygesen A, Oddershede J, Lilholt H, Thomsen A B, Ståhl K. On the determination of crystallinity and cellulose content in plant fibres. *Cellulose*, 2005, 12(6): 563–576